High-rate field demonstration of large-alphabet quantum key distribution

Catherine Lee,[1,2] Darius Bunander,[1] Zheshen Zhang,[1]
Gregory R. Steinbrecher,[1,2] P. Ben Dixon,[1] Franco N. C. Wong,[1]
Jeffrey H. Shapiro,[1] Scott A. Hamilton,[2] Dirk Englund[1*]

[1]Research Laboratory of Electronics, Massachusetts Institute of Technology,
Cambridge, MA 02139, USA

[2]Lincoln Laboratory, Massachusetts Institute of Technology,
Lexington, MA 02420, USA

[*]To whom correspondence should be addressed; E-mail: englund@mit.edu.

May 22, 2017

A central goal of quantum information science is to transfer quantum states with high fidelity, efficiency, and speed. While the majority of quantum communications uses photons encoded in binary quantum states, it has recently been shown that high-dimensionally encoded states can provide significant advantages in applications such as quantum metrology and quantum communication. In particular, high-dimensional quantum key distribution enables higher secret-key generation rates under practical limitations of detectors or light sources, as well as greater error tolerance. Here, we demonstrate the first high-dimensional quantum key distribution field test, using photons encoded in a high-dimensional alphabet to increase the secure information yield per de-

tected photon. By adjusting the alphabet size, it is possible to optimize secret-key rate for different channel loss scenarios. These demonstrations enable record quantum secure communication rates over metro-scale distances and mark an important step toward high-speed transmission of high-dimensional quantum states in deployed fiber networks.

Introduction

Quantum key distribution (QKD) allows two parties, Alice and Bob, to establish provably secure encryption keys at a distance. The keys can be used with encryption schemes like the one-time pad (OTP), which requires no assumptions about the computational abilities of an adversary. QKD commonly relies on the transmission and detection of single photons to distribute the secret keys, but the secret-key generation rates are often limited by the receiver hardware, which caps the achievable photon detection rate (*1*). Under this constraint, for a given maximum detection rate, the secret-key rate can still be raised by optimizing the photonic encoding. The first QKD schemes used photons encoded in two states, such as two different polarization states (*2, 3*). Recently, much effort has turned to large-alphabet QKD schemes, which encode photons in a larger set of high-dimensional basis states (*4–12*). Compared to binary-encoded QKD, such large-alphabet schemes can encode more secure information per detected photon, boosting secure communication rates, and also provide increased resilience to noise and loss (*13*). High-dimensional encoding may also improve the efficiency of quantum sensing (*14*) and other tasks in quantum information processing, such as performing Bell tests (*15*) and implementing quantum gates (*16*). We take advantage of high-dimensional encoding to demonstrate a record QKD rate for three different channel losses using a prepare-and-measure high-speed, large-alphabet QKD protocol, including the first field demonstration of large-alphabet QKD in a deployed-fiber testbed.

High-dimensional encoding is possible in a variety of degrees of freedom, and large-alphabet QKD has been demonstrated in the laboratory using position-momentum (*8*), time-energy (*5, 6, 9–11*), and orbital angular momentum modes (*7, 12*). Of these, time-energy encoding is appealing for its compatibility with existing telecommunications infrastructure — which lowers the barriers to widespread adoption of QKD. The time-energy correlations are robust over transmission in both fiber and free-space channels and are preserved when passing through wavelength-division multiplexing.

In high-dimensional temporal encoding, the position of a photon within a symbol frame comprising M time slots can convey as much as $\log_2 M$ bits of information, as depicted in Figure 1(a). Classically, this encoding is known as pulse position modulation (PPM), and combined with single-photon detection, it achieves near-optimal performance in terms of bits per detected photon (*17*). Assuming a constant slot duration, PPM exhibits a trade-off between the alphabet size M and the transmitted symbol rate: an increase in the former directly corresponds to a decrease in the latter. The alphabet size determines how much information is encoded in each photon, and the transmitted symbol rate directly affects how many photons are received per second. We take advantage of this trade-off to maximize the secret-key rate in the presence of receiver saturation.

Figure 1(b) is a representative plot of secret-key rate versus channel length for binary encoding with realizable parameters. Three regimes of distance/loss are indicated. In normal operation (Region II), the secret-key rate decreases exponentially with distance until the received photon flux is comparable to the background counts of the detector(s). At distances/losses beyond this cutoff point (Region III), the correlations between sender and receiver are masked by the background and the secret-key rate drops abruptly. However, at short distances, i.e., low losses (Region I), the secret-key rate is limited when some component of the receiver hardware — such as the detectors or the readout electronics — is saturated by the incoming photon flux,

as illustrated in Figure 1(b). In this regime, which extends to approximately 100 km for these parameters, the best strategy to maximize the secret-key rate is to reduce the transmitted photon rate by increasing the alphabet size until the receiver is just below saturation. Although much research has focused on extending the range of QKD links well beyond 100 km (*18–21*), deployed QKD networks will include a variety of link lengths with potentially different optimal technologies, and thus we focus here on using high-dimensional encoding to maximize secret-key rates over metropolitan-area distances of tens of kilometers.

Results

To demonstrate high-rate, large-alphabet QKD, we implemented dispersive-optics QKD (DO-QKD) (*22*), a high-dimensional QKD protocol based on time-energy encoding, with the basis transformations produced by group velocity dispersion (GVD). We previously proved the security of this scheme against arbitrary collective attacks (*22*) and implemented the scheme using entangled photon pairs in the laboratory (*10*). The present work is a prepare-and-measure (P&M) version of DO-QKD, with decoy-state protection against photon number splitting attacks (*23–25*).

In P&M DO-QKD, as pictured in Figure 2, the transmitter, Alice, filters a broadband light source to $\sim$ 25 GHz centered at 1559 nm and uses an electro-optic modulator to encode a PPM sequence that will become the raw key. To prepare in the time basis, Alice sends the PPM pulse to the receiver, Bob, and to prepare in the energy basis, she applies normal GVD with magnitude 10,000 ps/nm to the pulse before sending it to Bob. The basis choice must be random to an eavesdropper, Eve, but known to Alice. Before transmitting, Alice attenuates the pulses to keep the average number of photons less than one per pulse, but she varies the intensity between signal states, which are used for generating secure keys, and weaker decoy states, which are used for channel monitoring to guard against a photon-number-splitting attack.

Alice also precompensates for the GVD incurred over the fiber channel, or the security of the protocol would be degraded. On a separate channel (not pictured in Figure 2), Alice sends a periodic, bright optical pulse that Bob detects with a photodiode and uses as a timing reference. To measure in the time basis, Bob detects the photon arrival time, and to measure in the energy basis, he applies anomalous GVD with magnitude 10,000 ps/nm to the photon before detecting the arrival time. Bob's single-photon detectors are niobium nitride (NbN) SNSPDs capable of counting at hundreds of Mcps rates, with 68% detection efficiency, timing resolution of tens of picoseconds, and few kcps dark count rates (*26*). A single optical fiber is coupled to four interleaved nanowires, which are read out by a commercial time-to-digital converter (Picoquant Hydraharp 400) with a 80 ns dead time per channel. Information can be shared when Alice and Bob both apply GVD or both do not apply GVD. When only one party applies GVD, the correlation between prepared pulse time and measured pulse time is degraded from tens of picoseconds (limited by the detector timing resolution) to nanoseconds (determined by the optical bandwidth and the magnitude of the GVD). After the photon timetags are recorded, Alice and Bob convert the photon timing correlations into shared secret keys through a series of classical postprocessing steps. Bob demodulates the PPM signal, and Alice and Bob sift their data to postselect symbols encoded and decoded using the same basis. They correct errors between their symbol strings using a multi-layer low-density parity-check (LDPC) code (*27*), and they perform privacy amplification to eliminate Eve's information about their shared error-free symbol strings.

The secure photon information efficiency (PIE) quantifies Alice and Bob's information advantage over Eve, who can mount arbitrary collective attacks. In the asymptotic regime, the secure PIE for DO-QKD with decoy-state analysis is

$$r_{\infty,\mathrm{decoy}} = \beta I(A;B) - (1 - F_{\mu}^{\mathrm{LB}}) \log_2 M - F_{\mu}^{\mathrm{LB}} \chi^{\mathrm{UB}}(A;E), \tag{1}$$

where $\beta I(A;B)$ is Alice and Bob's reconciled mutual information, F_μ^{LB} is a lower bound on the fraction of Bob's detection events that came from a single-photon transmission by Alice, and $\chi^{\mathrm{UB}}(A;E)$ is an upper bound on Eve's Holevo information (*22, 25, 28*). By measuring the covariance matrix associated with the correlation between prepared pulse time and measured pulse time (*22, 28*) and by monitoring the quantum channel using weak-intensity decoy states (*23–25*), Alice and Bob can bound $\chi^{\mathrm{UB}}(A;E)$, the information accessible to Eve. Any information that Alice and Bob share in excess of this bound will be secure, except with a finite failure probability that corresponds to the predetermined security parameter ε_s (*29–32*).

Decoy state measurements contribute to the estimation of F_μ^{LB} and $\chi^{\mathrm{UB}}(A;E)$. In the finite-key regime, we must consider the effects of a finite sample size on the estimation of the parameters related to decoy states (*32*), in addition to the standard finite-size effects on parameter estimation, error correction, and privacy amplification (*31*).

We tested the system, varying the PPM alphabet size $M \in \{4, 8, 16, 32\}$, in three scenarios: in the laboratory in the back-to-back configuration with negligible channel loss, in the laboratory using a 41-km spool of standard single-mode fiber, and in a field test over a 43-km deployed fiber. The deployed-fiber testbed comprised a pair of dark fibers running between the main campus of MIT in Cambridge, MA, and MIT Lincoln Laboratory in Lexington, MA, as illustrated in Figure 2. Installed fibers are subject to environmental perturbations, such as temperature fluctuations, that are not present in the laboratory, as well as higher losses due to greater numbers of splices and bends. The 41-km fiber spool had a total loss of 7.6 dB, but the loss over the deployed fiber was 12.7 dB — equivalent to 63.5 km of standard single-mode fiber on a spool (assuming standard loss of 0.2 dB/km).

In the back-to-back configuration, we observed a maximum secret-key rate of 23 Mbps with $M = 16$. Over the 41-km fiber spool, the maximum secret-key rate was 5.3 Mbps with $M = 8$. Over the 43-km deployed fiber, the maximum secret-key rate was 1.2 Mbps with

$M = 4$. Table 1 summarizes the three test cases, and Figure 3(a) plots the experimental results along with theoretical secret-key rates as functions of channel loss. The reported values and theoretical curves include decoy state and finite-key analysis with sample size $N = 10^9$ counts and security parameter $\varepsilon_s = 10^{-10}$ (*31, 32*). Colors correspond to alphabet size and thus to test configuration, since each configuration had a different optimal alphabet size. The theoretical curves were computed using the experimental conditions, such as detector timing jitter and the measured timing correlations, which were not the same for all three test configurations. Thus, we cannot directly compare the three curves to determine the universally optimal alphabet size for a given loss. Instead, Figure 3(b) displays the secret-key rates obtained for each alphabet size in the three test cases.

The optimal M to maximize the secret-key rate depends most strongly on Bob's received photon rate, which is in turn a function of channel loss. If Bob had an ideal receiver, the highest secret-key rate would be obtained for the fastest transmitter rate, which occurs for $M = 2$. However, Bob's receiver hardware is usually rate-limited. The limit may be due to the single-photon detectors themselves; for instance, SNSPDs exhibit reset times ranging from a few nanoseconds (*26, 33–35*) to several tens of nanoseconds (*35–37*), depending on the choice of superconductor. The detector readout electronics can also limit the receiver count rate, as is the case for the commercial time-tagger in our system. When Bob's receivable photon rate is limited, increasing $M > 2$ allows Alice and Bob to effectively produce secret keys even during the reset time. Thus, at short distances and correspondingly low losses, we can expect a bottleneck due to the maximum count rate of Bob's receiver. In this receiver-limited regime, it is advantageous to increase M to encode as much information as possible in each detected photon while keeping the receiver just below saturation, and indeed, Figure 3(b) demonstrates that the optimal M decreases as channel loss increases.

Our measurements do not consider the case when $M = 2$ because DO-QKD is not op-

timal when $M = 2$. The secure PIE presented in Eq. 1 holds only against the class of collective attacks, whereas traditional, two-dimensional protocols such as the Bennett-Brassard 1984 (BB84) protocol (*2*) have proven security against the most general, coherent attacks (*38*). Futhermore, Eq. 1 tends to yield a lower secure PIE than that afforded by BB84. Ref (*38*), the highest-rate BB84 demonstration for which secure PIE data is available, obtained 0.26 bit/photon with 10 dB channel loss. At the same loss, a numerical simulation shows that P&M DO-QKD with $M = 2$ achieves a secure PIE of 0.16 bit/photon. The numerical simulation uses the measured parameters (e.g., Alice and Bob's timing correlations, detector timing jitter) of the deployed-fiber test case. Over the deployed fiber with 12.7 dB loss, DO-QKD with $M = 2$ should achieve a secret-key rate of 605 kbps, indicating that increasing M provides a boost in the secret-key rate.

Discussion

The 1.2 Mbps secret-key rate over the deployed fiber is the highest rate reported to date in a QKD field test and also compares favorably to previously published high-rate laboratory demonstrations under similar losses (*1,38*). Additionally, Figure 4 plots our results along with a variety of notable QKD experiments (*1, 11, 20, 39–41*). Our results show an improvement over other works for channel losses in the range of 0–15 dB. Our secret-key rate advantage comes from both the high-dimensional QKD protocol, which effectively generates secure information even during the receiver's dead time, taking advantage of what would be wasted time for traditional two-dimensional protocols. A slower receiver would amplify the inherent advantage of the high-dimensional protocol, as saturation would occur at lower incoming photon rates.

The high-dimensional time-energy encoding demonstrated here offers the ability to optimize the secret-key rate by varying the alphabet size M in response to both channel loss and receiver limitations. This is particularly useful when Bob's detectors are saturated, which often occurs

over metropolitan-area distances of tens of kilometers. By presenting and demonstrating a protocol intended to adapt to the constraints of a particular link implementation, this work represents a new approach to high-rate secure quantum communication optimized for use in metropolitan areas.

Materials and Methods

The deployed-fiber testbed comprised a pair of dark fibers, one of which is used for quantum signals, and the other of which is used for bright synchronization pulses. Alice's light source was a superluminescent diode with tens of nanometers of optical bandwidth. This source can enable DO-QKD with multiple spectral channels, although this demonstration used only one channel with 25 GHz of optical bandwidth, filtered by a tunable bandpass filter. The 25 GHz output was modulated by an electro-optic modulator with a PPM sequence of 50 ps pulses centered in 240 ps time slots that was produced by a pulse pattern generator (PPG). The resulting optical pulses were attenuated to either $\mu = 0.5$ photons/pulse for signal states or $\nu = 0.05$ photons/pulse for decoy states. A circulator at the output of Alice's transmitter (not pictured in Fig. 2) provided some protection against a Trojan horse attack. The bright synchronization pulse was produced by a continuous-wave laser modulated by an electro-optic modulator driven by another output of the same PPG. The synchronization pulse period was a constant multiple of the symbol frame length. In the back-to-back and spool tests, the period was 256 times the symbol frame length for all M. For the deployed-fiber test, the period was reduced to 64 times the symbol frame length to mitigate the effects of timing drifts over the installed fiber.

Following the signal exchange and measurement step, the classical postprocessing — error reconcilation and privacy amplification — was performed offline. Because only one SNSPD system was available, Bob could not randomly choose between the two measurement bases. Therefore, we fixed both Alice and Bob's basis selections for the duration of each data ac-

quisition period. The resulting datasets were combined in postprocessing. For each test case, numerical optimization of the secret-key rate determined the probabilities with which Alice and Bob should have selected each basis; the data from different bases were combined using these probabilities to compute the reported experimental secret-key rates. Similarly, Alice's choice of signal or decoy intensity was fixed for the duration of each acquisition period, the probabilities with which Alice selected signal or decoy states were determined by numerical optimization for each test case, and the data from different intensities were combined using these probabilities in postprocessing.

References

1. L. C. Comandar, *et al.*, *Appl. Phys. Lett.* **104**, 021101 (2014).

2. C. H. Bennett, G. Brassard, *Proceedings of IEEE International Conference on Computers, Systems, and Signal Processing* (IEEE, New York, 1984), pp. 175–179.

3. C. H. Bennett, F. Bessete, G. Brassard, L. Salvail, J. Smolin, *Journal of Cryptology* **5**, 3 (1992).

4. H. Bechmann-Pasquinucci, W. Tittel, *Phys. Rev. A* **61**, 062308 (2000).

5. W. Tittel, J. Brendel, H. Zbinden, N. Gisin, *Phys. Rev. Lett.* **84**, 4737 (2000).

6. I. Ali-Khan, C. J. Broadbent, J. C. Howell, *Phys. Rev. Lett.* **98**, 060503 (2007).

7. M. Mafu, *et al.*, *Phys. Rev. A* **88**, 032305 (2013).

8. S. Etcheverry, *et al.*, *Sci. Rep.* **3**, 2316 (2013).

9. J. Nunn, *et al.*, *Opt. Express* **21**, 15959 (2013).

10. C. Lee, *et al.*, *Phys. Rev. A* **90**, 062331 (2014).

11. T. Zhong, *et al.*, *New J. Phys.* **17**, 022002 (2015).

12. M. Mirhosseini, *et al.*, *New J. Phys.* **17**, 033033 (2015).

13. N. J. Cerf, M. Bourennane, A. Karlsson, N. Gisin, *Phys. Rev. Lett.* **88**, 127902 (2002).

14. R. Fickler, *et al.*, *Science* **338**, 640 (2012).

15. A. C. Dada, J. Leach, G. S. Buller, M. J. Padgett, E. Andersson, *Nat. Phys.* **7**, 677 (2011).

16. B. P. Lanyon, *et al.*, *Nat. Phys.* **5**, 134 (2009).

17. B. S. Robinson, *et al.*, *Opt. Lett.* **31**, 444 (2006).

18. D. Stucki, *et al.*, *New J. Phys.* **11**, 075003 (2009).

19. S. Wang, *et al.*, *Opt. Lett.* **37**, 1008 (2012).

20. B. Korzh, *et al.*, *Nat. Photon.* **9**, 163 (2015).

21. B. Fröhlich, *et al.*, *Optica* **4**, 163 (2017).

22. J. Mower, *et al.*, *Phys. Rev. A* **87**, 062322 (2013).

23. X.-B. Wang, *Phys. Rev. Lett.* **94**, 230503 (2005).

24. H.-K. Lo, X. Ma, K. Chen, *Phys. Rev. Lett.* **94**, 230504 (2005).

25. D. Bunandar, Z. Zhang, J. H. Shapiro, D. R. Englund, *Phys. Rev. A* **91**, 022336 (2015).

26. D. Rosenberg, A. J. Kerman, R. J. Molnar, E. A. Dauler, *Opt. Express* **21**, 1440 (2013).

27. H. Zhou, L. Wang, G. Wornell, *Proc. Information Theory and Applications Workshop (ITA), 2013* (IEEE, Piscataway, NJ, 2013), pp. 1–10.

28. Z. Zhang, J. Mower, D. Englund, F. N. C. Wong, J. H. Shapiro, *Phys. Rev. Lett.* **112**, 120506 (2014).

29. V. Scarani, R. Renner, *Phys. Rev. Lett.* **100**, 200501 (2008).

30. A. Leverrier, F. Grosshans, P. Grangier, *Phys. Rev. A* **81**, 062343 (2010).

31. C. Lee, J. Mower, Z. Zhang, J. Shapiro, D. Englund, *Quantum Inf. Process.* **14**, 1005 (2015).

32. H. Bao, W. Bao, Y. Wang, C. Zhou, R. Chen, *J. Phys. A: Mathematical and Theoretical* **49**, 205301 (2016).

33. A. J. Kerman, *et al.*, *Appl. Phys. Lett.* **88**, 111116 (2006).

34. A. J. Kerman, D. Rosenberg, R. J. Molnar, E. A. Dauler, *Journal of Applied Physics* **113**, 144511 (2013).

35. E. A. Dauler, *et al.*, *Opt. Eng.* **53**, 081907 (2014).

36. F. Marsili, *et al.*, *Nat. Photon.* **7**, 210 (2013).

37. R. Valivarthi, *et al.*, *Opt. Express* **22**, 24497 (2014).

38. M. Lucamarini, *et al.*, *Opt. Express* **21**, 24550 (2013).

39. L. C. Comandar, *et al.*, *Nat. Photon.* **10**, 312 (2016).

40. D. Huang, P. Huang, D. Lin, G. Zeng, *Sci. Rep.* **6**, 19201 (2016).

41. A. Treiber, *et al.*, *New J. Phys.* **11**, 045013 (2009).

	Back-to-back	41-km spool	43-km deployed fiber
Loss (dB)	0.1	7.6	12.7
Slot duration (ps)	240	240	240
Optimal M	16	8	4
Max. secret-key rate (bps)	23×10^6	5.3×10^6	1.2×10^6
Secure PIE (bit/photon)	1.40	0.88	0.50
Symbol-error-rate (SER)	0.065	0.048	0.049

Table 1: Summary of the maximum secret-key rates obtained in the three test cases.

Acknowledgments

DISTRIBUTION STATEMENT A: Approved for public release: distribution unlimited.

This material is based upon work supported by the Assistant Secretary of Defense for Research and Engineering under Air Force Contract No. FA8721-05-C-0002 and/or FA8702-15-D-0001. Any opinions, findings, conclusions or recommendations expressed in this material are those of the author(s) and do not necessarily reflect the views of the Assistant Secretary of Defense for Research and Engineering.

D.E. and D.B. acknowledge partial support from the Air Force Office of Scientific Research Multidisciplinary University Research Initiative (FA9550-14-1-0052) and the Air Force Research Laboratory RITA program (FA8750-14-2-0120). D.B. also acknowledges support from the Samsung Advanced Institute of Technology. **General:** C.L. thanks David O. Caplan and Nivedita Chandrasekaran for helpful discussions. **Author contributions:** C.L. and D.B. built the setup and collected the data, with guidance and supervision from Z.Z., P.B.D., S.A.H., and D.E. C.L. analyzed the data using code written by G.R.S. and C.L. D.B. performed additional security analysis. D.E., J.H.S, F.N.C.W., Z.Z., and C.L. devised the protocol. C.L., D.E., and P.B.D. wrote the manuscript with contributions from the other authors. **Competing interests:** The authors declare that they have no competing interests.

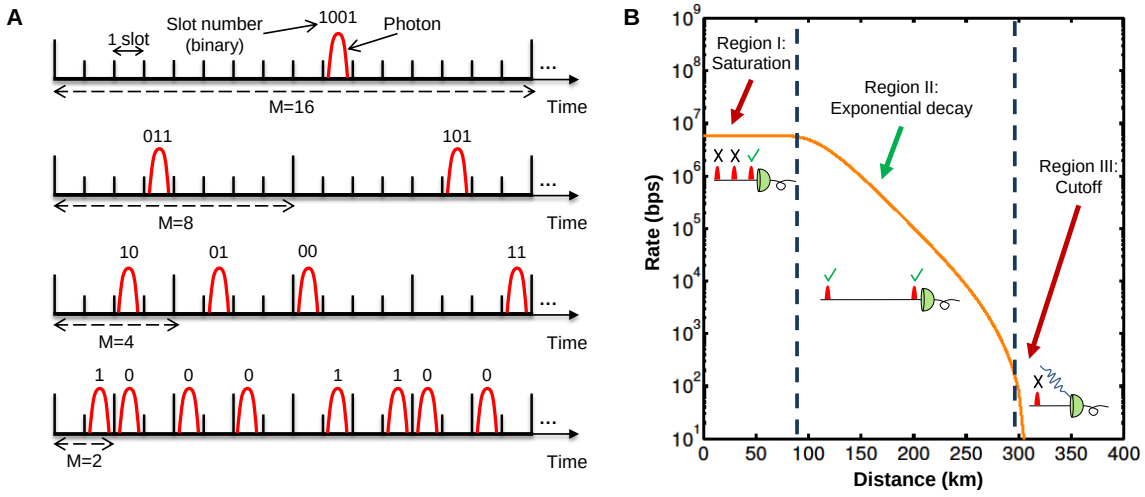

Figure 1: (a) In high-dimensional temporal encoding (pulse position modulation), information is encoded in the position of an optical pulse within M slots, depicted here for alphabet size $M \in \{2, 4, 8, 16\}$. For a fixed slot duration, the alphabet size and the transmitted pulse rate are inversely proportional. (b) Representative plot of secret-key rate versus channel length for a traditional two-dimensional QKD protocol, assuming a 5 Gbps modulation rate, a 0.2 dB/km channel loss, a 1 kcps background count rate, a 93% detector efficiency, and a 100 ns detector reset time after each detection event. Three regions are denoted: I. At short distances, 0-100 km (or correspondingly, low losses, 0-20 dB), the secret-key rate is limited by detector saturation. II. For higher losses (normal operation), the secret-key rate decays exponentially with distance. III. At even higher losses ($>$ 300 km), a cutoff is reached when Bob's received photon rate becomes comparable to his detectors' background count rate. The error rate grows and the secret-key rate drops abruptly.

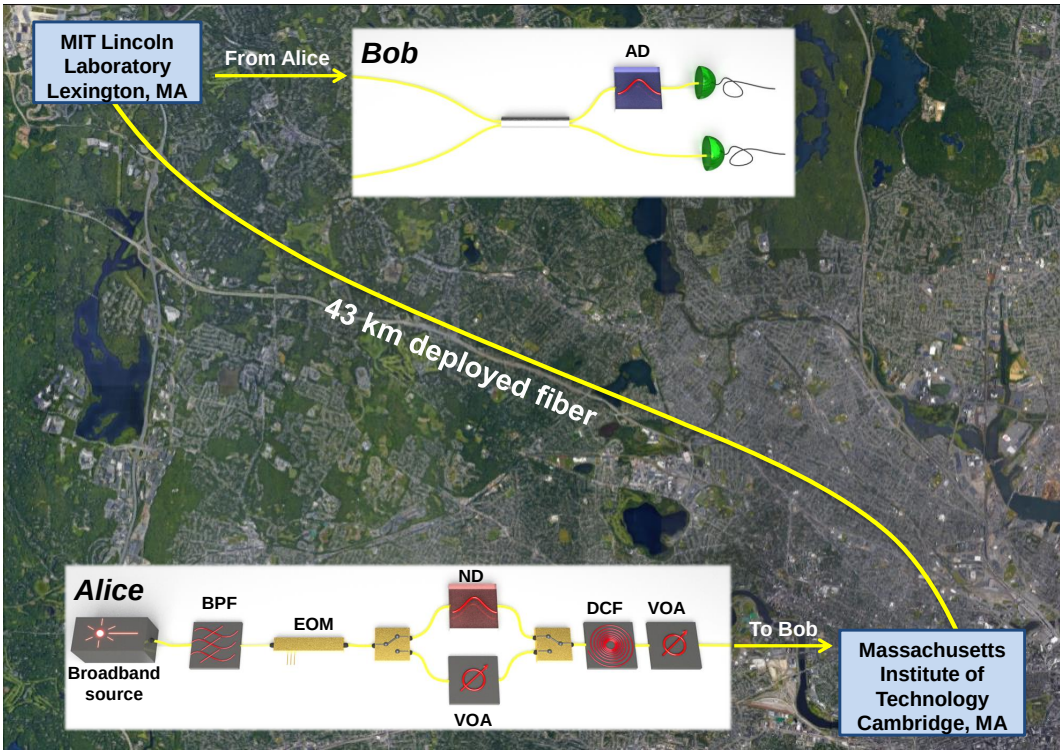

Figure 2: Map showing node locations and approximate path of the installed 43-km deployed-fiber testbed used in this work. Overlaid are Alice's transmitter, located in Cambridge, MA, and Bob's receiver, located in Lexington, MA. BPF: bandpass filter. EOM: electro-optic modulator. VOA: variable attenuator. ND: normal GVD. AD: anomalous GVD. DCF: dispersion-compensating fiber.

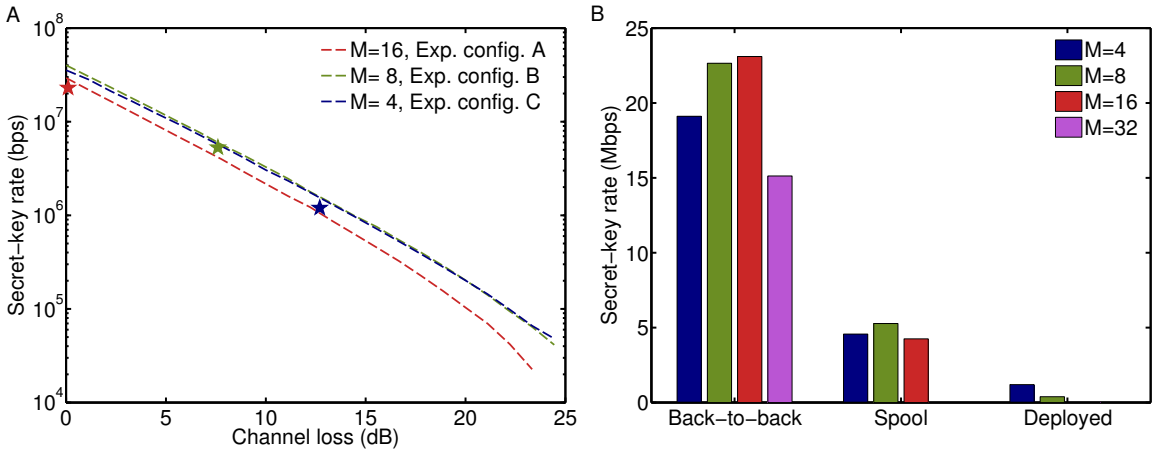

Figure 3: (a) Experimental (stars) and theoretical (dashed curves) secret-key rates versus channel loss. Colors correspond to optimal alphabet size M for each of the three test configurations. Each theoretical curve uses a different set of experimental parameters (e.g., detector timing jitter) that corresponds to each of the test configurations: Exp. config A = Back-to-back; exp. config. B = spool; exp. config. C = deployed fiber. (b) Experimental secret-key rates for all alphabet sizes of each test case. Loss increases from left to right. The optimal M decreases as loss increases. For experimental convenience, we did not increase the alphabet size once it became apparent that doing so would not increase the secret-key rate.

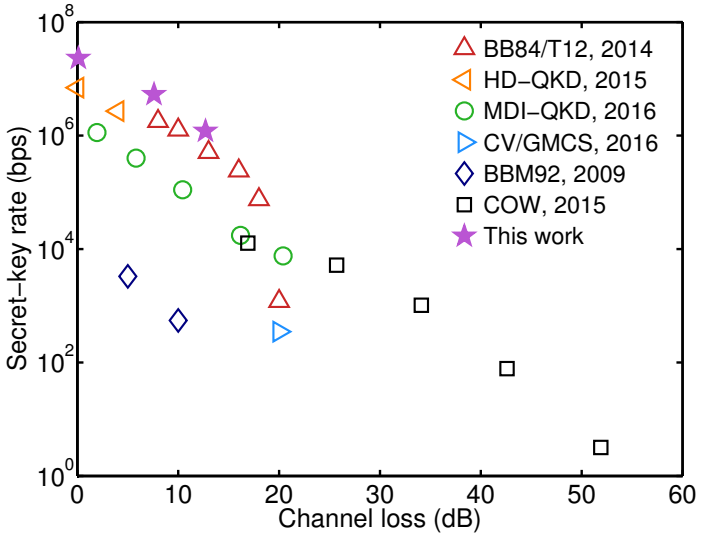

Figure 4: Comparison of our P&M DO-QKD results to previously published QKD system records, chosen to represent either secure throughput or distance records for a variety of protocols. BB84/T12: secure throughput record for two-dimensional QKD (*1*). HD-QKD: secure throughput record for high-dimensional entanglement-based QKD (*11*). MDI-QKD: secure throughput record for measurement-device-independent QKD (*39*). CV/GMCS: distance record for continuous-variable QKD (*40*). BBM92: secure throughput record for two-dimensional entanglement-based QKD (*41*). COW: distance record for QKD (*20*).